

DDFV scheme for nonlinear parabolic reaction-diffusion problems on general meshes

Bazirha Z., Azrar L.

Research Center STIS, M2CS, Department of Applied Mathematics and Informatics, ENSAM, Mohammed V University, Rabat, Morocco

(Received 26 June 2023; Revised 2 February 2024; Accepted 3 February 2024)

This paper focuses on the nonlinear anisotropic parabolic model of the form $\partial_t C(u) - \operatorname{div}(\Lambda \nabla u) + R(u) = f$, where C , R , f , and Λ are respectively: two nonlinear functions, a source term and an anisotropic tensor diffusion. For space discretization, various types of the Discrete Duality Finite Volume (DDFV) scheme are elaborated leading to positive definite stiffness matrices for the diffusion term. A general mesh is used and hard anisotropic tensor with discontinuous effects is considered. An implicit time scheme is developed as well as the Newton–Raphson method to solve the resulting nonlinear system. An iterative incremental approach is elaborated handling the effects of anisotropy, discontinuity and non-linearity. The performance of the presented direct and indirect DDFV schemes for different meshes has been demonstrated by various numerical tests. A super-convergence in the discrete L^2 and H^1 -norms is also demonstrated.

Keywords: *nonlinear parabolic reaction–diffusion problems; anisotropic tensor; DDFV; Newton–Raphson method.*

2010 MSC: 65Hxx, 65N08, 65N22, 65Mxx, 65M50 **DOI:** 10.23939/mmc2024.01.096

1. Introduction

In this paper, the study and focus are on a finite volume method on the associated rectangular and triangular meshes for a nonlinear parabolic diffusion-reaction problem (\mathcal{P}) defined as follows:

$$(\mathcal{P}) = \begin{cases} \partial_t C(u) - \operatorname{div}(\Lambda(x) \nabla u) + R(u) = f(x, t) & \text{on } Q_T = (0, T) \times \Omega, \\ u(x, t) = 0 & \text{on } (0, T) \times \partial\Omega, \\ u(x, 0) = u_0(x) & \text{in } \Omega. \end{cases} \quad (1)$$

Hypotheses (H)

H_1 : C is continuous and strictly increasing function with $C(0) = 0$.

H_2 : $\forall x \in \Omega \subset \mathbb{R}^2, \forall \xi \in \mathbb{R}^2 \bar{\Lambda}_{\min} |\xi|^2 \leq \Lambda(x) \xi \cdot \xi \leq \bar{\Lambda}_{\max} |\xi|^2$ with $0 < \bar{\Lambda}_{\min} \leq \bar{\Lambda}_{\max}$.

H_3 : $u_0 \in L^\infty(\Omega)$.

H_4 : $f \in L^\infty(\Omega_T)$.

H_5 : we take the same assumption in [1] for the nonlinear function R .

The problem (\mathcal{P}) arises in many scientific fields, such as flow in anisotropic porous media, plasma physics, chemistry and reservoir simulations. The unknown function u and the function C can represent water pressure and water content respectively. The Λ matrix is a possibly anisotropic and heterogeneous diffusion tensor. The function R represents chemical reactions, and f is the source term. In the simulation of geological basins and reservoirs, the standard finite volume method cannot be applied, as the orthogonality condition defined in [2] is not verified and the diffusion tensor may be anisotropic. This is why many authors are interested in developing a finite volume method that handles anisotropic effects, distorted meshes and non-linear effects. To take advantage of the cheap implementation of the classical finite volume method, several contributions have analyzed the diffusion problem [3–5]. Several numerical methods have been applied to the equation (1), for example the finite element method [6–8] and the finite volume method [9–11].

In this work, the emphasis is on the DDFV (Discrete Duality Finite Volume) method introduced for the Laplace equation in [12] and developed by numerous authors. In [13], it was proved that DDFV is equivalent to a non-conforming finite element approach for the Laplace equation, for the diffusion equation in the context of domain decomposition [14], the convection–diffusion problem [15, 16], the Maxwell’s equations [17], the Stokes and Navier–Stokes equation [18, 19] and for linear or nonlinear elliptic problems of the Leray–Lions type [20–22].

The DDFV method uses unknowns on the centers and at the vertices unlike classical finite volume uses unknowns on the centers. With a larger number of unknowns, we can approximate the gradient in the whole diamond [18], or in the half diamond [23] and on the quarter diamond [21].

On one hand, super-convergence is a common phenomenon in the finite volume method. Numerical results can be found in [13] for the Laplace equation with a special refinement of triangular meshes. General quadrilateral meshes with convex and concave elements for the diffusion equation, where the diffusion tensor can be anisotropic and discontinuous, super-convergence is obtained in [23]. On the other hand, in this paper, we will test the refinement strategy for rectangular mesh presented in [23], for the nonlinear parabolic reaction-diffusion equation in rectangular and triangular associated meshes using different DDFV schemes.

This document is structured as follows: First, we give some notations to clarify and simplify the DDFV framework. In section 2, we will present different DDFV meshes with two ways of constructing the dual mesh. The discrete gradient and the divergence operator in the half-diamond will also be defined. Section 3 will focus on the approximation of equations (1), while in the discretization of space, various DDFV schemes will be used and an implicit Euler time discretization will also be considered. The last section is devoted to analyzing the accuracy of various DDFV schemes in several tests. Different meshes with convex and concave elements, strongly anisotropic tensor diffusion, discontinuous and nonlinear effects will be taken into account. The resulting nonlinear system is solved using the Newton–Raphson method.

Remark 1. The weak solution of the problem (\mathcal{P}) is presented in [1], with some assumptions for the function R and here the same proof for uniqueness in [24] can be adapted.

Notations

- $x_{\mathcal{K}}$: centroid of \mathcal{K} .
- σ : primal edge.
- $x_{\mathcal{K}^*}$: center of \mathcal{K}^* .
- $m_{\mathcal{K}}$: measure of \mathcal{K} .
- \mathcal{E} : set of edges of the primal mesh
- \mathcal{E}_{int} : set of interior edges of the primal mesh.
- \mathcal{E}_{ext} : set of boundary edges of the primal mesh.
- $\mathcal{E}_{\mathcal{K}}$: set of edges of \mathcal{K}
- m_{σ} : length of σ .
- $x_{\mathcal{K}^*}$: centroid of \mathcal{K}^* .
- σ^* : dual edge.
- $m_{\mathcal{K}^*}$: measure of \mathcal{K}^* .
- \mathcal{E}^* : set of edges of the dual mesh.
- $\mathcal{E}_{\mathcal{K}^*}$: set of edges of $\mathcal{K}^* \in \mathcal{M}^*$.
- $\mathcal{E}_{\text{int}}^*$: set of interior edges of the dual mesh.
- x_{σ^*} : middle point of the edges σ^* .
- m_{σ^*} : length of σ^* .
- $\vec{n}_{\sigma, \mathcal{K}}$: the unit normal to σ outwards \mathcal{K} .
- $\vec{n}_{\sigma^*, \mathcal{K}^*}$: the unit normal to σ^* outwards \mathcal{K}^* .
- $m_{\mathcal{D}}$: the measure of the diamond $\mathcal{D}_{\sigma, \sigma^*}$.
- \mathcal{D} : set of all diamonds.
- $\mathcal{D}_{\mathcal{K}} = \{\mathcal{D}_{\sigma, \sigma^*} \in \mathcal{D}, \sigma \in \mathcal{E}_{\mathcal{K}}\}$.
- $\mathcal{D}_{\mathcal{K}^*} = \{\mathcal{D}_{\sigma, \sigma^*} \in \mathcal{D}, \sigma^* \in \mathcal{E}_{\mathcal{K}^*}\}$.
- $\widetilde{\sigma}^* = \widetilde{\sigma}_{\mathcal{K}}^*$ or $\widetilde{\sigma}_{\mathcal{L}}^*$, with $\widetilde{\sigma}_{\mathcal{K}}^* = [x_{\mathcal{K}}, x_{\sigma}]$ and $\widetilde{\sigma}_{\mathcal{L}}^* = [x_{\sigma}, x_{\mathcal{L}}]$.
- $\alpha_{\mathcal{K}}$ or $\alpha_{\mathcal{L}}$: angle between σ and $\widetilde{\sigma}^*$ in $]0, \frac{\pi}{2}[$.
- $\widetilde{\mathcal{D}}$: set of all half-diamonds.
- $\widetilde{\mathcal{D}}$ or $\widetilde{\mathcal{D}}_{\sigma, \mathcal{K}}$: half-diamond associated with the polygon \mathcal{K} .
- $\widetilde{\mathcal{D}}_{\mathcal{K}^*} = \{\widetilde{\mathcal{D}}_{\sigma, \mathcal{K}} \in \widetilde{\mathcal{D}}, \widetilde{\sigma}_{\mathcal{K}}^* \in \mathcal{E}_{\mathcal{K}^*}\}$.
- $\widetilde{\mathcal{D}}_{\mathcal{K}} = \{\widetilde{\mathcal{D}}_{\sigma, \mathcal{K}} \in \widetilde{\mathcal{D}}, \sigma \in \mathcal{E}_{\mathcal{K}}\}$.
- $\vec{n}_{\widetilde{\sigma}_{\mathcal{K}^*}^*, \mathcal{K}^*}$: the unit normal to $\widetilde{\sigma}_{\mathcal{K}^*}^*$ outwards \mathcal{K}^* .
- $\vec{n}_{\widetilde{\sigma}_{\mathcal{L}^*}^*, \mathcal{K}^*}$: the unit normal to $\widetilde{\sigma}_{\mathcal{L}^*}^*$ outwards \mathcal{K}^* .
- \mathcal{D}_{ext} : set of boundary diamonds.
- \mathcal{D}_{int} : set of interior diamonds.

2. DDFV framework

2.1. DDFV meshes

Discretization in context of DDFV requires three meshes: A primal mesh denoted by \mathcal{M} is a set of the union disjoint polygon \mathcal{K} recover the whole domaine $\bar{\Omega}$ such as: $\bar{\Omega} = \sqcup_{\mathcal{K} \in \Omega} \bar{\mathcal{K}}$ and $\forall \mathcal{K}, \mathcal{L} \ \mathcal{L} \cap \mathcal{K} = \emptyset$ with \mathcal{K} and \mathcal{L} are neighboring volumes. For given polygons \mathcal{K} is not necessary convex and the center of gravity maybe outside of \mathcal{K} , so we choose $x_{\mathcal{K}}$ be inside \mathcal{K} (case: concave quadrilateral element [23]). We note by $\sigma = \mathcal{K}|\mathcal{L} = (x_{\mathcal{K}^*}, x_{\mathcal{L}^*}) \in \mathcal{E}_{\text{int}}$ the internal edges of primal mesh, otherwise $\sigma \in \mathcal{E}_{\text{ext}}$ if $\sigma \in \partial\Omega$ is boundary primal edges.

The dual mesh will be constructed in two ways. The first way is by joining all centroid $x_{\mathcal{K}}$ directly as presented in Figure 1. Second way is by connecting the centroid $x_{\mathcal{K}}$ with midpoints of each primal edge σ of \mathcal{K} denoted by x_{σ} see Figure 2, where $x_{\sigma} = \sigma \cap \sigma^*$ in the first case. We designate by \mathcal{M}^* the dual mesh in two cases. By the same way $\sigma^* = \mathcal{K}^*|\mathcal{L}^* = (x_{\mathcal{K}}, x_{\mathcal{L}}) \in \mathcal{E}_{\text{int}}^*$ is the internal edges of the dual mesh.

The quadrilateral diamond cell \mathcal{D} or $\mathcal{D}_{\sigma, \sigma^*}$, defined by the primal edge σ and the dual edge σ^* which are here diagonal. The vertices of $\mathcal{D}_{\sigma, \sigma^*}$ are $(x_{\mathcal{K}}, x_{\mathcal{L}}, x_{\mathcal{K}^*}, x_{\mathcal{L}^*})$. Note that the diamond is the union of the disjoint triangles $(x_{\mathcal{K}}, x_{\mathcal{K}^*}, x_{\mathcal{L}^*})$ and $(x_{\mathcal{L}}, x_{\mathcal{K}^*}, x_{\mathcal{L}^*})$ see Figures 1–2, the two triangles construct the two half-diamond such as: $\mathcal{D}_{\sigma, \sigma^*} = \tilde{\mathcal{D}}_{\sigma, \mathcal{K}} \cup \tilde{\mathcal{D}}_{\sigma, \mathcal{L}}$. Furthermore, if $\sigma \in \mathcal{E}_{\text{ext}}$, the quadrilateral $\mathcal{D}_{\sigma, \sigma^*}$ is degenerate and becomes a triangle as presented in Figure 3. The set of all diamond and half-diamond are denoted respectively by \mathfrak{D} and $\tilde{\mathfrak{D}}$ such as:

$$\bar{\Omega} = \sqcup_{\mathcal{D} \in \mathfrak{D}} \bar{\mathcal{D}} = \sqcup_{\tilde{\mathcal{D}}_{\sigma, \mathcal{K}} \in \tilde{\mathfrak{D}}} \overline{\tilde{\mathcal{D}}_{\sigma, \mathcal{K}}}.$$

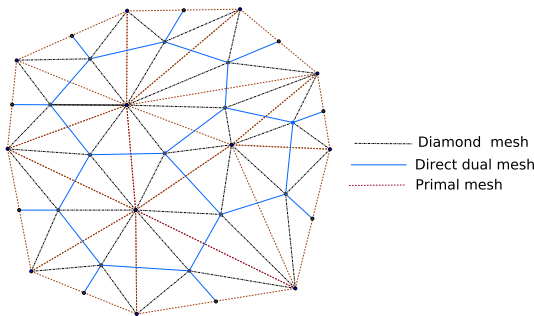


Fig. 1. DDFV meshes with direct way to construct the dual mesh.

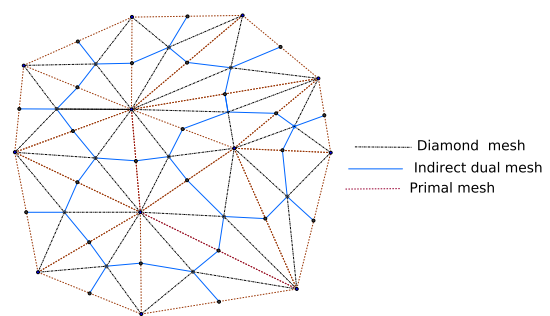


Fig. 2. DDFV meshes with indirect way to construct the dual mesh.

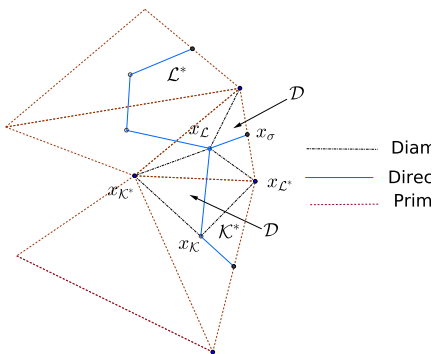


Fig. 3. Boundary meshes.

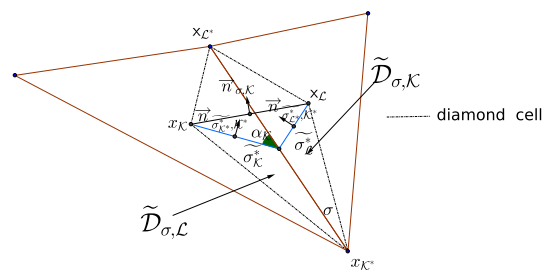


Fig. 4. Notations for two half-diamonds.

The approximate solution $u^{\mathcal{T}}$ is defined as $u^{\mathcal{T}} \in \mathbb{R}^{\mathcal{T}} \Leftrightarrow u^{\mathcal{T}} = ((u_{\mathcal{K}})_{\mathcal{K} \in \mathcal{M}}, (u_{\mathcal{K}^*})_{\mathcal{K}^* \in \mathcal{M}^*})$. Such as:

$$u_{\mathcal{K}} = \frac{1}{m_{\mathcal{K}}} \int_{\mathcal{K}} u(x) dx \quad \text{and} \quad u_{\mathcal{K}^*} = \frac{1}{m_{\mathcal{K}^*}} \int_{\mathcal{K}^*} u(x) dx.$$

2.2. Discrete operators in the half-diamond

We define the discrete gradient in half-diamond as follow:

$$\nabla_{\sigma,\mathcal{K}}^{\tilde{\mathcal{D}}} u^{\mathcal{T}} = \frac{1}{\sin(\alpha_{\mathcal{K}})} \left(\frac{(u_{\sigma} - u_{\mathcal{K}})}{m_{\tilde{\sigma}_{\mathcal{K}}^*}} \mathbf{n}_{\sigma,\mathcal{K}} + \frac{(u_{\mathcal{L}^*} - u_{\mathcal{K}^*})}{m_{\sigma}} \mathbf{n}_{\tilde{\sigma}_{\mathcal{K}^*}^*,\mathcal{K}^*} \right),$$

where

$$2m_{\tilde{\mathcal{D}}_{\sigma,\mathcal{K}}} = m_{\sigma} m_{\tilde{\sigma}_{\mathcal{K}}^*} \sin(\alpha_{\mathcal{K}}). \quad (2)$$

Using (2) (see Figure 4) we will give an explicit expression for the discrete gradient and divergence in the half-diamond:

Definition 1 (Discrete gradient on half-diamond). Let $u^{\mathcal{T}} \in \mathbb{R}^{\mathcal{T}}$, we assume $\nabla^{\tilde{\mathcal{D}}} u^{\mathcal{T}} = (\nabla^{\tilde{\mathcal{D}}} u^{\mathcal{T}})_{\tilde{\mathcal{D}} \in \tilde{\mathcal{D}}}$ and we define the discrete gradient as follows: $\nabla^{\tilde{\mathcal{D}}}: \mathbb{R}^{\mathcal{T}} \mapsto (\mathbb{R}^2)^{\tilde{\mathcal{D}}}$ such as on the half-diamonds $\tilde{\mathcal{D}}_{\sigma,\mathcal{K}}$ and $\tilde{\mathcal{D}}_{\sigma,\mathcal{L}}$ are defined by:

$$\begin{aligned} \nabla_{\sigma,\mathcal{L}}^{\tilde{\mathcal{D}}} u^{\mathcal{T}} &= \frac{1}{2 \times m_{\tilde{\mathcal{D}}_{\sigma,\mathcal{L}}}} \left(m_{\sigma} (u_{\sigma} - u_{\mathcal{L}}) \mathbf{n}_{\sigma,\mathcal{L}} + m_{\tilde{\sigma}_{\mathcal{L}^*}^*} (u_{\mathcal{L}^*} - u_{\mathcal{K}^*}) \mathbf{n}_{\tilde{\sigma}_{\mathcal{L}^*}^*,\mathcal{K}^*} \right), \\ \nabla_{\sigma,\mathcal{K}}^{\tilde{\mathcal{D}}} u^{\mathcal{T}} &= \frac{1}{2 \times m_{\tilde{\mathcal{D}}_{\sigma,\mathcal{K}}}} \left(m_{\sigma} (u_{\sigma} - u_{\mathcal{K}}) \mathbf{n}_{\sigma,\mathcal{K}} + m_{\tilde{\sigma}_{\mathcal{K}^*}^*} (u_{\mathcal{L}^*} - u_{\mathcal{K}^*}) \mathbf{n}_{\tilde{\sigma}_{\mathcal{K}^*}^*,\mathcal{K}^*} \right). \end{aligned}$$

Remark 2. $m_{\sigma^*} \mathbf{n}_{\sigma^*,\mathcal{K}^*} = m_{\tilde{\sigma}_{\mathcal{K}^*}^*} \mathbf{n}_{\tilde{\sigma}_{\mathcal{K}^*}^*,\mathcal{K}^*} + m_{\tilde{\sigma}_{\mathcal{L}^*}^*} \mathbf{n}_{\tilde{\sigma}_{\mathcal{L}^*}^*,\mathcal{K}^*}$.

Definition 2 (Discrete divergence on half-diamond). The discrete divergence operator is defined as follows:

$$\operatorname{div}^{\mathcal{T}}(\nabla^{\tilde{\mathcal{D}}} u^{\mathcal{T}}) = \left(\operatorname{div}^{\mathfrak{M}}(\nabla^{\tilde{\mathcal{D}}} u^{\mathcal{T}}), \operatorname{div}^{\partial\mathfrak{M}}(\nabla^{\tilde{\mathcal{D}}} u^{\mathcal{T}}), \operatorname{div}^{\mathfrak{M}^*}(\nabla^{\tilde{\mathcal{D}}} u^{\mathcal{T}}), \operatorname{div}^{\partial\mathfrak{M}^*}(\nabla^{\tilde{\mathcal{D}}} u^{\mathcal{T}}) \right)$$

with $\operatorname{div}^{\mathfrak{M}}(\nabla^{\tilde{\mathcal{D}}} u^{\mathcal{T}}) = (\operatorname{div}_{\mathcal{K}}(\nabla^{\tilde{\mathcal{D}}} u^{\mathcal{T}}))_{\mathcal{K} \in \mathfrak{M}}$, $\operatorname{div}^{\partial\mathfrak{M}}(\nabla^{\tilde{\mathcal{D}}} u^{\mathcal{T}}) = 0$, $\operatorname{div}^{\mathfrak{M}^*}(\nabla^{\tilde{\mathcal{D}}} u^{\mathcal{T}}) = (\operatorname{div}_{\mathcal{K}^*}(\nabla^{\tilde{\mathcal{D}}} u^{\mathcal{T}}))_{\mathcal{K}^* \in \mathfrak{M}^*}$, $\operatorname{div}^{\partial\mathfrak{M}^*}(\nabla^{\tilde{\mathcal{D}}} u^{\mathcal{T}}) = (\operatorname{div}_{\mathcal{K}^*}(\nabla^{\tilde{\mathcal{D}}} u^{\mathcal{T}}))_{\mathcal{K}^* \in \partial\mathfrak{M}^*}$,

$$\forall \mathcal{K} \in \mathfrak{M} \quad \operatorname{div}_{\mathcal{K}}(\nabla^{\tilde{\mathcal{D}}} u^{\mathcal{T}}) = \frac{1}{m_{\mathcal{K}}} \sum_{\sigma \in \mathcal{E}_{\mathcal{K}}} m_{\sigma} \nabla_{\sigma,\mathcal{K}}^{\tilde{\mathcal{D}}} u^{\mathcal{T}} \cdot \mathbf{n}_{\sigma,\mathcal{K}},$$

$$\forall \mathcal{K}^* \in \mathfrak{M}^{\text{int}} \quad \operatorname{div}_{\mathcal{K}^*}(\nabla^{\tilde{\mathcal{D}}} u^{\mathcal{T}}) = \frac{1}{m_{\mathcal{K}^*}} \sum_{\sigma^* \in \mathcal{E}_{\mathcal{K}^*}} \left(m_{\tilde{\sigma}_{\mathcal{K}^*}^*} \nabla_{\sigma,\mathcal{K}}^{\tilde{\mathcal{D}}} u^{\mathcal{T}} \cdot \mathbf{n}_{\tilde{\sigma}_{\mathcal{K}^*}^*,\mathcal{K}^*} + m_{\tilde{\sigma}_{\mathcal{L}^*}^*} \nabla_{\sigma,\mathcal{L}}^{\tilde{\mathcal{D}}} u^{\mathcal{T}} \cdot \mathbf{n}_{\tilde{\sigma}_{\mathcal{L}^*}^*,\mathcal{K}^*} \right),$$

$$\begin{aligned} \forall \mathcal{K}^* \in \mathfrak{M}^{\text{ext}} \quad \operatorname{div}_{\mathcal{K}^*}(\nabla^{\tilde{\mathcal{D}}} u^{\mathcal{T}}) &= \frac{1}{m_{\mathcal{K}^*}} \left(\sum_{\sigma^* \in \mathcal{E}_{\mathcal{K}^*}} \left(m_{\tilde{\sigma}_{\mathcal{K}^*}^*} \nabla_{\sigma,\mathcal{K}}^{\tilde{\mathcal{D}}} u^{\mathcal{T}} \cdot \mathbf{n}_{\tilde{\sigma}_{\mathcal{K}^*}^*,\mathcal{K}^*} + m_{\tilde{\sigma}_{\mathcal{L}^*}^*} \nabla_{\sigma,\mathcal{L}}^{\tilde{\mathcal{D}}} u^{\mathcal{T}} \cdot \mathbf{n}_{\tilde{\sigma}_{\mathcal{L}^*}^*,\mathcal{K}^*} \right) \right. \\ &\quad \left. + \sum_{\sigma^* \in \mathcal{E}_{\mathcal{K}^*} \cap \partial\Omega} \frac{m_{\sigma}}{2} \nabla_{\sigma,\mathcal{K}}^{\tilde{\mathcal{D}}} u^{\mathcal{T}} \cdot \mathbf{n}_{\sigma,\mathcal{K}} \right). \end{aligned}$$

3. DDFV schemes for parabolic reaction-diffusion equation

The discrete duality finite volume procedure will be applied to the nonlinear parabolic reaction-diffusion equation (1). Each term will be discretized in time and space.

3.1. Approximation of the diffusion term

By integrating the diffusion term over \mathcal{K} and applying Green's formula, lead to:

$$\begin{aligned} - \int_{\mathcal{K}} \operatorname{div}(\Lambda \nabla u(x)) dx &= - \int_{\partial\mathcal{K}} \Lambda \nabla u(s) \cdot \mathbf{n}_{\sigma,\mathcal{K}} ds \\ &= - \sum_{\sigma \in \mathcal{E}_{\mathcal{K}}} \int_{\sigma} \Lambda \nabla u(s) \cdot \mathbf{n}_{\sigma,\mathcal{K}} ds. \end{aligned}$$

The primal flux $-\Lambda \nabla u(s) \cdot \mathbf{n}_{\sigma, \mathcal{K}}$ is approximated by:

$$-\Lambda^{\tilde{\mathcal{D}}_{\sigma, \mathcal{K}}} \nabla_{\sigma, \mathcal{K}}^{\tilde{\mathcal{D}}} u^T \cdot \mathbf{n}_{\sigma, \mathcal{K}} = \mathbf{a}_{\mathcal{K}}^i (u_{\mathcal{K}} - u_{\sigma}) + \mathbf{b}_{\mathcal{K}}^i (u_{\mathcal{K}^*} - u_{\mathcal{L}^*}),$$

where

$$\Lambda^{\tilde{\mathcal{D}}_{\sigma, \mathcal{X}}} = \frac{1}{m_{\tilde{\mathcal{D}}_{\sigma, \mathcal{X}}}} \int_{\tilde{\mathcal{D}}_{\sigma, \mathcal{X}}} \Lambda(x) dx \quad \text{with } \mathcal{X} \in \{\mathcal{K}, \mathcal{L}\}.$$

Integrating now over \mathcal{K}^* leads with the same way to:

$$\begin{aligned} - \int_{\mathcal{K}^*} \operatorname{div}(\Lambda \nabla u(x)) dx &= - \int_{\partial \mathcal{K}^*} \Lambda \nabla u(s) \cdot \mathbf{n}_{\sigma^*, \mathcal{K}^*} ds \\ &= - \sum_{\sigma \in \mathcal{E}_{\mathcal{K}^*}} \int_{\sigma^*} \Lambda \nabla u(s) \cdot \mathbf{n}_{\sigma^*, \mathcal{K}^*} ds. \end{aligned}$$

For the dual flux $-\Lambda \nabla u(s) \cdot \mathbf{n}_{\sigma^*, \mathcal{K}^*}$ can be approximated by

$$- \sum_{\mathcal{X} \in \{\mathcal{K}, \mathcal{L}\}} m_{\sigma_{\mathcal{X}}^*} \Lambda^{\tilde{\mathcal{D}}_{\sigma, \mathcal{X}}} \nabla_{\sigma, \mathcal{X}}^{\tilde{\mathcal{D}}} u^T \cdot \mathbf{n}_{\sigma_{\mathcal{X}}^*, \mathcal{K}^*} = (\mathbf{c}_{\mathcal{K}}^i + \mathbf{c}_{\mathcal{L}}^i)(u_{\mathcal{K}^*} - u_{\mathcal{L}^*}) + \mathbf{b}_{\mathcal{K}}^i (u_{\mathcal{K}} - u_{\sigma}) + \mathbf{b}_{\mathcal{L}}^i (u_{\sigma} - u_{\mathcal{L}}),$$

such that

$$\begin{cases} \mathbf{a}_{\mathcal{X}}^i = \frac{\Lambda^{\tilde{\mathcal{D}}_{\sigma, \mathcal{X}}}}{2 \times m_{\tilde{\mathcal{D}}_{\sigma, \mathcal{X}}}} m_{\sigma} m_{\sigma} \mathbf{n}_{\sigma, \mathcal{K}} \cdot \mathbf{n}_{\sigma, \mathcal{K}}, \\ \mathbf{b}_{\mathcal{X}}^i = \frac{\Lambda^{\tilde{\mathcal{D}}_{\sigma, \mathcal{X}}}}{2 \times m_{\tilde{\mathcal{D}}_{\sigma, \mathcal{X}}}} m_{\sigma} m_{\sigma_{\mathcal{X}}^*} \mathbf{n}_{\sigma_{\mathcal{X}}^*, \mathcal{K}^*} \cdot \mathbf{n}_{\sigma, \mathcal{K}}, \\ \mathbf{c}_{\mathcal{X}}^i = \frac{\Lambda^{\tilde{\mathcal{D}}_{\sigma, \mathcal{X}}}}{2 \times m_{\tilde{\mathcal{D}}_{\sigma, \mathcal{X}}}} m_{\sigma_{\mathcal{X}}^*} m_{\sigma_{\mathcal{X}}^*} \mathbf{n}_{\sigma_{\mathcal{X}}^*, \mathcal{K}^*} \cdot \mathbf{n}_{\sigma_{\mathcal{X}}^*, \mathcal{K}^*}, \end{cases} \quad \text{with } \mathcal{X} \in \{\mathcal{K}, \mathcal{L}\},$$

u_{σ} is located at the point x_{σ} (x_{σ} is the middle point of the edges σ in this case).

Using the continuity condition at σ : $-A^{\tilde{\mathcal{D}}_{\sigma, \mathcal{K}}} \nabla_{\sigma, \mathcal{K}}^{\tilde{\mathcal{D}}} u^T \cdot \mathbf{n}_{\sigma, \mathcal{K}} = A^{\tilde{\mathcal{D}}_{\sigma, \mathcal{L}}} \nabla_{\sigma, \mathcal{L}}^{\tilde{\mathcal{D}}} u^T \cdot \mathbf{n}_{\sigma, \mathcal{L}}$, leads to the following expression of u_{σ} :

$$u_{\sigma} = \frac{\mathbf{a}_{\mathcal{K}}^i u_{\mathcal{K}} + \mathbf{a}_{\mathcal{L}}^i u_{\mathcal{L}}}{\mathbf{a}_{\mathcal{K}}^i + \mathbf{a}_{\mathcal{L}}^i} + \frac{\mathbf{b}_{\mathcal{K}}^i - \mathbf{b}_{\mathcal{L}}^i}{\mathbf{a}_{\mathcal{K}}^i + \mathbf{a}_{\mathcal{L}}^i} (u_{\mathcal{K}^*} - u_{\mathcal{L}^*}).$$

The local stiffness matrix of the diffusion problem can be written as follows:

$$D_i^{\text{loc}} = \begin{pmatrix} \frac{\mathbf{a}_{\mathcal{K}}^i \mathbf{a}_{\mathcal{L}}^i}{\mathbf{a}_{\mathcal{K}}^i + \mathbf{a}_{\mathcal{L}}^i} & \frac{\mathbf{a}_{\mathcal{K}}^i \mathbf{b}_{\mathcal{L}}^i + \mathbf{a}_{\mathcal{L}}^i \mathbf{b}_{\mathcal{K}}^i}{\mathbf{a}_{\mathcal{K}}^i + \mathbf{a}_{\mathcal{L}}^i} \\ \frac{\mathbf{a}_{\mathcal{K}}^i \mathbf{b}_{\mathcal{L}}^i + \mathbf{a}_{\mathcal{L}}^i \mathbf{b}_{\mathcal{K}}^i}{\mathbf{a}_{\mathcal{K}}^i + \mathbf{a}_{\mathcal{L}}^i} & \mathbf{c}_{\mathcal{K}}^i + \mathbf{c}_{\mathcal{L}}^i - \frac{(\mathbf{b}_{\mathcal{K}}^i - \mathbf{b}_{\mathcal{L}}^i)^2}{\mathbf{a}_{\mathcal{K}}^i + \mathbf{a}_{\mathcal{L}}^i} \end{pmatrix} = \begin{pmatrix} q_1^i & q_2^i \\ q_2^i & q_3^i \end{pmatrix}.$$

Where D_i^{loc} is calculated for a $\mathcal{D} \in \mathfrak{D}_{\text{int}}$, and if $\mathcal{D} \in \mathfrak{D}_{\text{ext}}$ the contribution D_i^{loc} is defined as follow:

$$D_i^{\text{loc}} = \begin{pmatrix} a_{\mathcal{K}}^i & b_{\mathcal{K}}^i \\ b_{\mathcal{K}}^i & c_{\mathcal{K}}^i \end{pmatrix} = \begin{pmatrix} q_1^i & q_2^i \\ q_2^i & q_3^i \end{pmatrix}.$$

By assembling these local contributions, we obtain a global stiffness matrix denoted by D_i .

If we suppose that the unknown u_{σ} is located at the point of intersection between σ and σ^* , and we replace $\mathbf{n}_{\sigma_{\mathcal{X}}^*, \mathcal{K}^*}$ by $\mathbf{n}_{\sigma^*, \mathcal{K}^*}$ in the formulas of $\mathbf{b}_{\mathcal{X}}^i$ and $\mathbf{c}_{\mathcal{X}}^i$, where $\mathcal{X} \in \{\mathcal{K}, \mathcal{L}\}$, we obtain the following expressions:

$$\begin{cases} \mathbf{b}_{\mathcal{X}}^d = \frac{\Lambda^{\tilde{\mathcal{D}}_{\sigma, \mathcal{X}}}}{2 \times m_{\tilde{\mathcal{D}}_{\sigma, \mathcal{X}}}} m_{\sigma} m_{\sigma_{\mathcal{X}}^*} \mathbf{n}_{\sigma^*, \mathcal{K}^*} \cdot \mathbf{n}_{\sigma, \mathcal{K}}, \\ \mathbf{c}_{\mathcal{X}}^d = \frac{\Lambda^{\tilde{\mathcal{D}}_{\sigma, \mathcal{X}}}}{2 \times m_{\tilde{\mathcal{D}}_{\sigma, \mathcal{X}}}} m_{\sigma_{\mathcal{X}}^*} m_{\sigma_{\mathcal{X}}^*} \mathbf{n}_{\sigma^*, \mathcal{K}^*} \cdot \mathbf{n}_{\sigma^*, \mathcal{K}^*}, \\ \mathbf{a}_{\mathcal{X}}^d = \mathbf{a}_{\mathcal{X}}^i, \end{cases} \quad \text{with } \mathcal{X} \in \{\mathcal{K}, \mathcal{L}\}.$$

Using the continuity condition at σ in the same way, we obtain the following explicit expression for u_{σ} :

$$u_{\sigma} = \frac{\mathbf{a}_{\mathcal{K}}^d u_{\mathcal{K}} + \mathbf{a}_{\mathcal{L}}^d u_{\mathcal{L}}}{\mathbf{a}_{\mathcal{K}}^d + \mathbf{a}_{\mathcal{L}}^d} + \frac{\mathbf{b}_{\mathcal{K}}^d - \mathbf{b}_{\mathcal{L}}^d}{\mathbf{a}_{\mathcal{K}}^d + \mathbf{a}_{\mathcal{L}}^d} (u_{\mathcal{K}^*} - u_{\mathcal{L}^*}).$$

If $\mathcal{D} \in \mathfrak{D}_{\text{int}}$, the expression for the local stiffness matrix of the diffusion problem is given by

$$D_d^{\text{loc}} = \begin{pmatrix} \frac{\mathbf{a}_{\mathcal{K}}^d \mathbf{a}_{\mathcal{L}}^d}{\mathbf{a}_{\mathcal{K}}^d + \mathbf{a}_{\mathcal{L}}^d} & \frac{\mathbf{a}_{\mathcal{K}}^d \mathbf{b}_{\mathcal{L}}^d + \mathbf{a}_{\mathcal{L}}^d \mathbf{b}_{\mathcal{K}}^d}{\mathbf{a}_{\mathcal{K}}^d + \mathbf{a}_{\mathcal{L}}^d} \\ \frac{\mathbf{a}_{\mathcal{K}}^d \mathbf{b}_{\mathcal{L}}^d + \mathbf{a}_{\mathcal{L}}^d \mathbf{b}_{\mathcal{K}}^d}{\mathbf{a}_{\mathcal{K}}^d + \mathbf{a}_{\mathcal{L}}^d} & \mathbf{c}_{\mathcal{K}}^d + \mathbf{c}_{\mathcal{L}}^d - \frac{(\mathbf{b}_{\mathcal{K}}^d - \mathbf{b}_{\mathcal{L}}^d)^2}{\mathbf{a}_{\mathcal{K}}^d + \mathbf{a}_{\mathcal{L}}^d} \end{pmatrix} = \begin{pmatrix} q_1^d & q_2^d \\ q_2^d & q_3^d \end{pmatrix}$$

For $\mathcal{D} \in \mathfrak{D}_{\text{ext}}$ the contribution D_d^{loc} is

$$D_d^{\text{loc}} = \begin{pmatrix} a_{\mathcal{K}}^d & b_{\mathcal{K}}^d \\ b_{\mathcal{K}}^d & c_{\mathcal{K}}^d \end{pmatrix} = \begin{pmatrix} q_1^d & q_2^d \\ q_2^d & q_3^d \end{pmatrix}.$$

By assembling the contribution of D_d^{loc} for all the diamonds, we obtain the global stiffness matrix denoted D_d .

Remark 3. Two matrices D_i and D_d are symmetric and positive definite as motioned and proved in [25].

3.2. Approximation to other terms

Our problem is time-dependent, so the discretization of the time interval $[0, T]$ is needed and given by $0 \leq t^1 < \dots < t^N = T$. The time step δt is supposed uniform such that $t^{n+1} - t^n = \delta t$. The first step consists in integrating each equation of problem (\mathcal{P}) over $]t^n, t^{n+1}] \times \mathcal{K}$:

$$\begin{aligned} \int_{t^n}^{t^{n+1}} \int_{\mathcal{K}} \partial_t C(u(x, t)) dx dt &\simeq m_{\mathcal{K}} (C_{\mathcal{K}}^{n+1} - C_{\mathcal{K}}^n) \quad \text{with} \quad C_{\mathcal{K}}^{n+1} = C(u_{\mathcal{K}}^{n+1}), \\ \int_{t^n}^{t^{n+1}} \int_{\mathcal{K}} f(x, t) dx dt &\simeq \delta t m_{\mathcal{K}} f_{\mathcal{K}}^{n+1} \\ \int_{t^n}^{t^{n+1}} \int_{\mathcal{K}} R(u(x, t)) dx dt &\simeq \delta t m_{\mathcal{K}} R_{\mathcal{K}}^{n+1}, \\ - \int_{t^n}^{t^{n+1}} \int_{\mathcal{K}} \text{div}(\Lambda \nabla u) dx dt &= - \sum_{\sigma \in \partial \mathcal{K}} \int_{t^n}^{t^{n+1}} \int_{\sigma} \Lambda \nabla u \cdot \mathbf{n}_{\sigma, \mathcal{K}} d\sigma dt \end{aligned}$$

with

$$- \int_{t^n}^{t^{n+1}} \int_{\sigma} \Lambda \nabla u \cdot \mathbf{n}_{\sigma, \mathcal{K}} d\sigma dt \simeq \delta t (q_1^x (u_{\mathcal{K}}^{n+1} - u_{\mathcal{L}}^{n+1}) + q_2^x (u_{\mathcal{K}^*}^{n+1} - u_{\mathcal{L}^*}^{n+1})) \quad \text{with} \quad x \in \{i, d\}.$$

These approximations lead to the following expression:

$$\frac{m_{\mathcal{K}} (C_{\mathcal{K}}^{n+1} - C_{\mathcal{K}}^n)}{\delta t} + \sum_{\mathcal{D}_{\sigma, \sigma^*} \in \mathfrak{D}_{\mathcal{K}}} F_{\sigma}^{n+1} + m_{\mathcal{K}} R_{\mathcal{K}}^{n+1} = m_{\mathcal{K}} f_{\mathcal{K}}^{n+1}, \quad \forall n \geq 0.$$

Using the same steps and integrating over $]t^n, t^{n+1}] \times \mathcal{K}^*$ lead to

$$\frac{m_{\mathcal{K}^*} (C_{\mathcal{K}^*}^{n+1} - C_{\mathcal{K}^*}^n)}{\delta t} + \sum_{\mathcal{D}_{\sigma, \sigma^*} \in \mathfrak{D}_{\mathcal{K}^*}} F_{\sigma^*}^{n+1} + m_{\mathcal{K}^*} R_{\mathcal{K}^*}^{n+1} = m_{\mathcal{K}^*} f_{\mathcal{K}^*}^{n+1}, \quad \forall n \geq 0.$$

Thus, the numerical scheme for the problem (\mathcal{P}) is

$$\begin{aligned} \frac{m_{\mathcal{K}} (C_{\mathcal{K}}^{n+1} - C_{\mathcal{K}}^n)}{\delta t} + \sum_{\mathcal{D}_{\sigma, \sigma^*} \in \mathfrak{D}_{\mathcal{K}}} F_{\sigma}^{n+1} + m_{\mathcal{K}} R_{\mathcal{K}}^{n+1} &= m_{\mathcal{K}} f_{\mathcal{K}}^{n+1} \quad \forall \mathcal{K} \in \mathcal{M}, \quad \forall n \geq 0, \\ \frac{m_{\mathcal{K}^*} (C_{\mathcal{K}^*}^{n+1} - C_{\mathcal{K}^*}^n)}{\delta t} + \sum_{\mathcal{D}_{\sigma, \sigma^*} \in \mathfrak{D}_{\mathcal{K}^*}} F_{\sigma^*}^{n+1} + m_{\mathcal{K}^*} R_{\mathcal{K}^*}^{n+1} &= m_{\mathcal{K}^*} f_{\mathcal{K}^*}^{n+1} \quad \forall \mathcal{K}^* \in \mathcal{M}^*, \quad \forall n \geq 0, \end{aligned}$$

where $F_{\sigma}^{n+1} = q_1^x (u_{\mathcal{K}}^{n+1} - u_{\mathcal{L}}^{n+1}) + q_2^x (u_{\mathcal{K}^*}^{n+1} - u_{\mathcal{L}^*}^{n+1})$ and $F_{\sigma^*}^{n+1} = q_2^x (u_{\mathcal{K}}^{n+1} - u_{\mathcal{L}}^{n+1}) + q_3^x (u_{\mathcal{K}^*}^{n+1} - u_{\mathcal{L}^*}^{n+1})$, $x \in \{i, d\}$ indicate that we use direct or indirect dual meshes. For the direct dual mesh, the scheme will be noted D-DDFV and for indirect will be it denoted by I-DDFV.

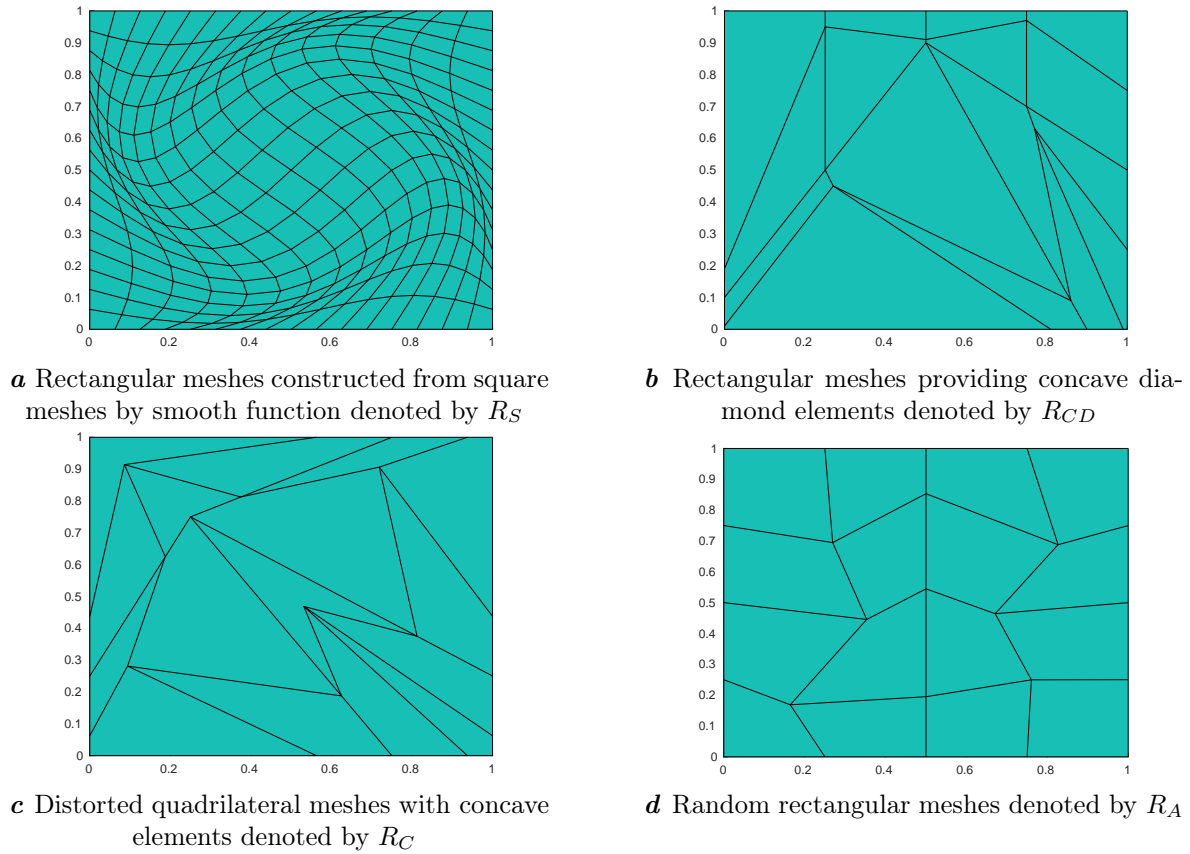


Fig. 5. Used meshes.

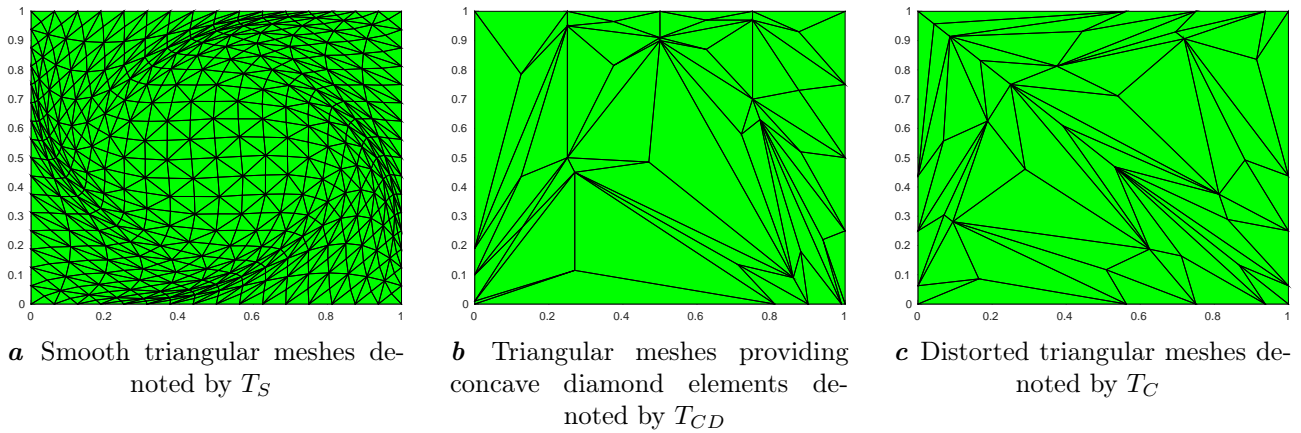


Fig. 6. Used triangular meshes.

4. Numerical results

In this section, errors and convergence rates in several numerical tests with known analytical solution are used to analyze the accuracy of the elaborated DDFV methodological approach. This method has been developed on general convex and concave quadrilateral meshes and associated triangular meshes. The discrete norms L^2 , H^1 and the convergence rate are defined as follows:

$$ER_{L^2} := \left(\sum_{\mathcal{K} \in \mathcal{M}} m_{\mathcal{K}} |u_{\text{exact}}(x_{\mathcal{K}}, T) - u(x_{\mathcal{K}}, T)|^2 + \sum_{\mathcal{K}^* \in \mathcal{M}^*} m_{\mathcal{K}^*} |u_{\text{exact}}(x_{\mathcal{K}^*}, T) - u(x_{\mathcal{K}^*}, T)|^2 \right)^{1/2},$$

$$ER_{H^1} := \left(\sum_{\mathcal{D}_{\sigma, \sigma^*} \in \mathcal{D}} m_{\mathcal{D}} |(\nabla_{\sigma, \mathcal{L}}^{\tilde{\mathcal{D}}} + \nabla_{\sigma, \mathcal{K}}^{\tilde{\mathcal{D}}})(u_{\text{exact}}(x_{\mathcal{K}}, T) - u(x_{\mathcal{K}}, T))|^2 \right)^{1/2},$$

$$\text{OR}_X := \frac{\log((\text{ER}_X)_i/(\text{ER}_X)_{i-1})}{\log((\delta_h)_i/(\delta_h)_{i-1})} \quad \text{with } X \in \{\text{ER}_{H^1}, \text{ER}_{L^2}\},$$

where T is the final time, $(\delta_h)_i$ and $(\delta_h)_{i-1}$ corresponding the sizes of two successive meshes.

A numerical code was developed in Matlab to generate the convex and concave meshes shown in Figures 5a–5d. To analyze the errors and convergence rates in several numerical tests the quadrilateral meshes in Figures 5b–5d are refined with the procedure presented in [23]. The associated triangular meshes are obtained by dividing each quadrilateral element into four triangles, as shown in Figures 6a–6c. In all tests, the expression of the nonlinear function C is $C(u) = u^3 + u$. For the exact solution u , the diffusion tensor Λ and the nonlinear function R will be given in each test. For the Dirichlet boundary data, initial condition $u_0(x)$ and the source term f are determined accordingly. The computational domain in this work is fixed to the unit square $\bar{\Omega} = [0, 1]^2$. The time discretization δt is equal to $T \times (\delta_h)^2$, where δ_h is space discretization such that $\delta_h = \max_{\sigma \in \mathcal{E}} m_\sigma$. The number of unknowns denoted by N_I is calculated as follow: $N_I = \text{number of cells} + \text{number of interior dual cells}$.

The resulting nonlinear system from the numerical scheme can be expressed like $\mathbb{F}(U^k) = 0$. Otherwise, the resolution of the nonlinear system by Newton–Raphson method, require to find the solution of the linear system of the form:

$$J(U^k) \delta U^k = -\mathbb{F}(U^k),$$

where $\delta U^k = U^{k+1} - U^k$ and the Jacobian matrix is $J(U^k)$. The stopped criterion is chosen as follows

$$\|\delta U^k\| \leq 10^{-8}.$$

Based on the presented methodological approach a numerical code has been elaborated for anisotropic media and various nonlinear function R and C . Various direct and indirect DDFV meshes may be used.

4.1. Test 1

In the first test, a non-polynomial function is considered for the exact solution with expression: $u(x, y, t) = (1 + \cos(\pi x))(5t)$ also taken in [26], with the tensor diffusion, reaction term and final time are respectively:

$$\Lambda(x, y) = \begin{pmatrix} 0.1 & 0 \\ 0 & 10 \end{pmatrix}, \quad R(u) = u^3, \quad \text{and } T = 0.2.$$

The mesh in Figure 5a is obtained by a smooth transformation of the square mesh and the numerical results in this mesh and it is associated triangular mesh presented in Figure 6a are shown in Tables 1 and 2. These tables show the second-order convergence rates in discrete L^2 -norm and greater than 1.7 in the discrete H^1 -norm for the two schemes. The rate of convergence in the discrete H^1 -norm on the triangular mesh is slightly greater than that on the rectangular mesh, as shown in Tables 3–4. For linear diffusion equation, the D-DDFV scheme is the first-order in the discrete L^2 -norm in a mesh providing a concave diamond element such as the meshes in Figures 5b and 6b [23]. In contrast, in the Tables 3 and 4, both schemes retain the second-order convergence in the discrete L^2 -norm. This may be due to the nonlinear effects.

Table 1. Test 1: Rate of convergence and errors in rectangular meshes R_S .

Scheme	δ_h	N_I	ER_{L^2}	ER_{H^1}	OR_{L^2}	OR_{H^1}
I-DDFV	0.5312	41	2.212e-01	1.517e+00	–	–
	0.3073	145	6.065e-02	5.715e-01	2.3635	1.7837
	0.1648	545	1.542e-02	1.838e-01	2.1968	1.8201
	0.0837	2113	3.781e-03	5.273e-02	2.0398	1.8422
D-DDFV	0.5312	41	2.169e-01	1.606e+00	–	–
	0.3073	145	5.994e-02	6.110e-01	2.3494	1.7656
	0.1648	545	1.528e-02	1.893e-01	2.1928	1.8798
	0.0837	2113	3.837e-03	5.339e-02	2.0391	1.8676

Table 2. Test 1: Rate of convergence and errors in triangular meshes T_S .

Scheme	δ_h	N_I	ER_{L^2}	ER_{H^1}	OR_{L^2}	OR_{H^1}
I-DDFV	0.5312	105	2.011e-01	1.750e+00	–	–
	0.3073	401	5.717e-02	6.572e-01	2.2978	1.7896
	0.1648	1569	1.461e-02	2.018e-01	2.1892	1.8946
	0.0837	6209	3.674e-03	5.617e-02	2.0366	1.8868
D-DDFV	0.5312	105	2.572e-01	1.604e+00	–	–
	0.3073	401	6.987e-02	5.998e-01	2.3485	1.7964
	0.1648	1569	1.797e-02	1.900e-01	2.1768	1.8443
	0.0837	6209	4.528e-03	5.432e-02	2.0351	1.8476

Table 3. Test 1: Rate of convergence and errors in rectangular meshes R_{CD} .

Scheme	δ_h	N_I	ER_{L^2}	ER_{H^1}	OR_{L^2}	OR_{H^1}
I-DDFV	1.1700	41	1.743e-01	2.378e+00	–	–
	0.5850	145	4.822e-02	7.847e-01	1.8537	1.5999
	0.2925	545	1.299e-02	2.597e-01	1.8921	1.5952
	0.1463	2113	3.318e-03	7.625e-02	1.9693	1.7680
D-DDFV	1.1700	41	2.184e-01	1.896e+00	–	–
	0.5850	145	5.300e-02	7.105e-01	2.0427	1.4158
	0.2925	545	1.350e-02	2.392e-01	1.9733	1.5706
	0.1463	2113	3.396e-03	7.389e-02	1.9907	1.6948

Table 4. Test 1: Rate of convergence and errors in triangular meshes T_{CD} .

Scheme	δ_h	N_I	ER_{L^2}	ER_{H^1}	OR_{L^2}	OR_{H^1}
I-DDFV	1.1700	105	2.638e-01	3.909e+00	–	–
	0.5850	401	6.940e-02	1.120e+00	1.9263	1.8026
	0.2925	1569	1.765e-02	2.915e-01	1.9755	1.9424
	0.1463	6209	4.428e-03	8.124e-02	1.9947	1.8431
D-DDFV	1.1700	105	2.591e-01	2.177e+00	–	–
	0.5850	401	6.911e-02	8.564e-01	1.9062	1.3460
	0.2925	1569	1.763e-02	2.633e-01	1.9707	1.7018
	0.1463	6209	4.429e-03	7.624e-02	1.9932	1.7879

4.2. Test 2

The test presented in [27], is also considered herein for comparison. On the other hand, we take $T = 0.25$. Where the tensor diffusion is:

$$\Lambda(x, y) = \begin{pmatrix} 100 & 0 \\ 0 & 0.1 \end{pmatrix}.$$

The exact solution:

$$u(x, y, t) = \frac{\lambda_1(x - 0.5)^2 + \lambda_2(y - 0.5)^2}{1 - t},$$

where $\lambda_1 = \frac{1}{1600}$ and $\lambda_2 = \frac{1}{1.6}$, reaction term is $R(u) = \sin(u)$.

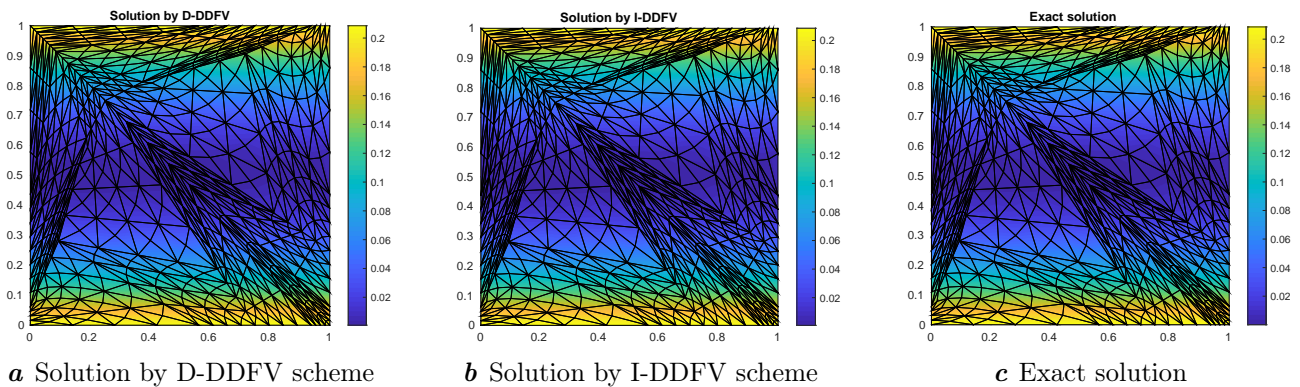
The considered exact solution is polynomial with nonlinear function in time t . Highly anisotropic tensor diffusion and very skewed mesh are considered herein. In triangular meshes the Figures 7a and 7b present solution profile by two schemes, and the obtained results are well compared to the exact solution as presented in Figure 7c. On the other hand, the refinement procedure presented in [23] allows us to obtain super-convergence in the discrete norms L^2 and H^1 without worrying about the presence of non-convex control volumes in the coarse mesh presented in Figure 5c for the problem (\mathcal{P}) , as shown in Tables 5 and 6. These tables also show that the order of convergence in the discrete H^1 -norm for the I-DDFV scheme is slightly higher than for the D-DDFV scheme.

Table 5. Test 2: Rate of convergence and errors in rectangular meshes R_C .

Scheme	δ_h	N_I	ER_{L^2}	ER_{H^1}	OR_{L^2}	OR_{H^1}
I-DDFV	0.9375	41	1.690e-02	2.885e-01	–	–
	0.4688	145	4.540e-03	1.279e-01	1.8958	1.1738
	0.2344	545	1.044e-03	5.304e-02	2.1208	1.2696
	0.1172	2113	2.417e-04	1.929e-02	2.1104	1.4590
D-DDFV	0.9375	41	1.688e-02	2.612e-01	–	–
	0.4688	145	4.551e-03	1.145e-01	1.8910	1.1898
	0.2344	545	1.046e-03	4.841e-02	2.1210	1.2420
	0.1172	2113	2.426e-04	1.855e-02	2.1085	1.3840

Table 6. Test 2: Rate of convergence and errors in triangular meshes T_C .

Scheme	δ_h	N_I	ER_{L^2}	ER_{H^1}	OR_{L^2}	OR_{H^1}
I-DDFV	0.9375	105	8.673e-03	1.123e-01	–	–
	0.4688	401	1.891e-03	4.532e-02	2.1975	1.3089
	0.2344	1569	4.723e-04	1.736e-02	2.0012	1.3843
	0.1172	6209	9.972e-05	5.498e-03	2.2438	1.6586
D-DDFV	0.9375	105	8.778e-03	9.272e-02	–	–
	0.4688	401	1.887e-03	3.983e-02	2.2179	1.2192
	0.2344	1569	4.658e-04	1.551e-02	2.0181	1.3602
	0.1172	6209	9.879e-05	5.184e-03	2.2374	1.5813

**Fig. 7.** Test 2: Exact solution and solution profile with D-DDFV and I-DDFV schemes with coarse mesh T_C .

4.3. Test 3

In the last test, discontinuous case for the exact solution and the tensor diffusion are considered and their expressions are given respectively as follow:

$$u(x, y, t) = \begin{cases} (\cos(\pi x) \sin(\pi y))t & \text{if } x \leq 0.5, \\ 0.01(\cos(\pi x) \sin(\pi y))t & \text{else,} \end{cases}$$

and

$$\Lambda(x, y) = \begin{cases} \begin{pmatrix} 1 & 0 \\ 0 & 1 \end{pmatrix} & \text{if } x \leq 0.5, \\ \begin{pmatrix} 100 & 0 \\ 0 & 0.01 \end{pmatrix} & \text{else,} \end{cases}$$

where $T = 1$ and $R(u) = u - u^2$.

The test considered herein is adapted for the problem (\mathcal{P}) from [28]. The mesh presented in Figure 5d is considered allowing the discontinuity in the line of equation $x = 0.5$, where the nodes located in this line are moved only in the y -direction. As presented in Figures 8a and 8b two schemes give similar solution profile compared to exact solution in Figure 8c. In this test, hard anisotropy with discontinuous tensor diffusion is considered. The obtained results given in Table 7 show the non-sensitivity of the order of convergence in the discrete L^2 and H^1 -norms, where are the second order convergence in the discrete L^2 -norm and greater than 1.7 in the discrete H^1 -norm.

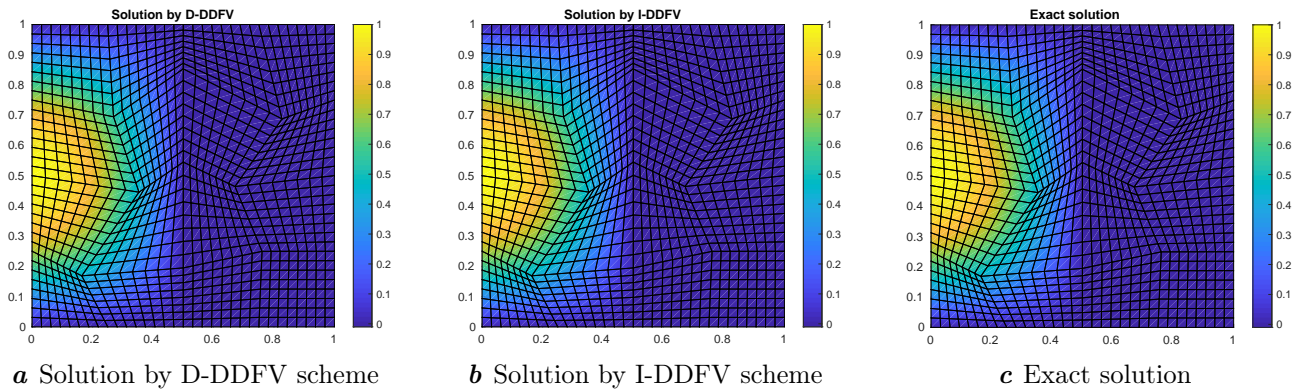


Fig. 8. Test 3: Exact solution and solution profile with D-DDFV and I-DDFV schemes with coarse mesh R_A .

Table 7. Test 3: Rate of convergence and errors in rectangular meshes R_A .

Scheme	δ_h	N_I	ER_{L^2}	ER_{H^1}	OR_{L^2}	OR_{H^1}
I-DDFV	1.5300	41	1.519e-02	2.152e-01	–	–
	0.7650	145	3.289e-03	5.951e-02	2.2077	1.8545
	0.3825	545	8.135e-04	1.721e-02	2.0156	1.7896
	0.1913	2113	2.031e-04	5.177e-03	2.0020	1.7333
D-DDFV	1.5300	41	1.359e-02	1.974e-01	–	–
	0.7650	145	2.924e-03	5.738e-02	2.2164	1.7822
	0.3825	545	7.163e-04	1.699e-02	2.0293	1.7559
	0.1913	2113	1.781e-04	5.154e-03	2.0080	1.7208

5. Conclusions & perspectives

In this paper, different DDFV meshes are presented: primal, dual and diamond meshes. The construction of the dual mesh with direct and indirect methods leads to different DDFV schemes called D-DDFV and I-DDFV respectively. Using discrete operators: gradient and divergence in the half-diamond, discretization for the diffusion term with various DDFV schemes are presented, where the resulting stiffness matrix is positive definite. For time discretization, an implicit Euler discretization is used, as well as the Newton–Raphson method for solving the resulting nonlinear system. Various numerical experiments are presented, to show the performance of the developed DDFV scheme for different distorted meshes, nonlinear, anisotropy and discontinuous effects. The super-convergence in the discrete L^2 and H^1 -norms is demonstrated in presence of anisotropy, distorted meshes and discontinuous tensor diffusion. As perspectives, we will develop a finite volume method for the degenerate parabolic convection–reaction–diffusion equation and Richard’s equation to achieve super-convergence in the discrete norms L^2 and H^1 . On the other hand, we will project this finite volume method to the Navier–Stokes problem.

-
- [1] Angelini O., Brenner K., Hilhorst D. A finite volume method on general meshes for a degenerate parabolic convection–reaction–diffusion equation. *Numerische Mathematik*. **123** (2), 219–257 (2013).
 - [2] Gallouët T., Herbin R., Vignal M. H. Error Estimates on the Approximate Finite Volume Solution of Convection Diffusion Equations with General Boundary Conditions. *SIAM Journal on Numerical Analysis*. **37** (6), 1935–1972 (2000).
 - [3] Aavatsmark I., Barkve T., Bøe O., Mannseth T. Discretization on unstructured grids for inhomogeneous, anisotropic media. Part II: Discussion and numerical results. *SIAM Journal on Scientific Computing*. **19** (5), 1717–1736 (1998).
 - [4] Eymard R., Gallouët T., Herbin R. A cell-centred finite-volume approximation for anisotropic diffusion operators on unstructured meshes in any space dimension. *IMA Journal of Numerical Analysis*. **26** (2), 326–353 (2006).

- [5] Faille I. A control volume method to solve an elliptic equation on a two-dimensional irregular mesh. *Computer Methods in Applied Mechanics and Engineering*. **100** (2), 275–290 (1992).
- [6] Arbogast T., Wheeler M. F. A nonlinear mixed finite element method for a degenerate parabolic equation arising in flow in porous media. *SIAM Journal on Numerical Analysis*. **33** (4), 1669–1687 (1996).
- [7] Dawson C. Analysis of an upwind-mixed finite element method for nonlinear contaminant transport equations. *SIAM Journal on Numerical Analysis*. **35** (5), 1709–1724 (1998).
- [8] Dawson C., Aizinger V. Upwind-mixed methods for transport equations. *Computational Geosciences*. **3**, 93–110 (1999).
- [9] Bessemoulin–Chatard M. A finite volume scheme for convection–diffusion equations with nonlinear diffusion derived from the Scharfetter–Gummel scheme. *Numerische Mathematik*. **121** (4), 637–670 (2012).
- [10] Afif M., Amaziane B. Convergence of finite volume schemes for a degenerate convection–diffusion equation arising in flow in porous media. *Computer Methods in Applied Mechanics and Engineering*. **191** (46), 5265–5286 (2002).
- [11] Eymard E., Hilhorst D., Vohralík M. A combined finite volume–finite element scheme for the discretization of strongly nonlinear convection–diffusion–reaction problems on nonmatching grids. *Numerical Methods for Partial Differential Equations: An International Journal*. **26** (3), 612–646 (2010).
- [12] Hermeline F. A finite volume method for the approximation of diffusion operators on distorted meshes. *Journal of Computational Physics*. **160** (2), 481–499 (2000).
- [13] Domelevo K., Omnes P. A finite volume method for the Laplace equation on almost arbitrary two-dimensional grids. *ESAIM: Mathematical Modelling and Numerical Analysis*. **39** (6), 1203–1249 (2005).
- [14] Belhadj H., Khallouq S., Rhoudaf M. Parallelization of a finite volumes discretization for anisotropic diffusion problems using an improved Schur complement technique. *Discrete and Continuous Dynamical Systems – S*. **14** (7), 2075–2099 (2021).
- [15] Baron V., Coudiere Y., Sochala P. Comparison of DDFV and DG methods for flow in anisotropic heterogeneous porous media. *Oil & Gas Science and Technology — Revue d’IFP Energies nouvelles*. **69**, 673–686 (2014).
- [16] Coudière Y., Manzini G. The discrete duality finite volume method for convection-diffusion problems. *SIAM Journal on Numerical Analysis*. **47** (6), 4163–4192 (2010).
- [17] Hermeline F., Layouni S., Omnes P. A finite volume method for the approximation of Maxwell’s equations in two space dimensions on arbitrary meshes. *Journal of Computational Physics*. **227** (22), 9365–9388 (2008).
- [18] Krell S. Stabilized DDFV schemes for stokes problem with variable viscosity on general 2d meshes. *Numerical Methods for Partial Differential Equations*. **27** (6), 1666–1706 (2011).
- [19] Goudon T., Krell S., Lissoni G. DDFV method for Navier–Stokes problem with outflow boundary conditions. *Numerische Mathematik*. **142** (1), 55–102 (2019).
- [20] Andreianov B., Boyer F., Hubert F. Discrete duality finite volume schemes for Leray–Lions–type elliptic problems on general 2D meshes. *Numerical Methods for Partial Differential Equations*. **23** (1), 145–195 (2007).
- [21] Boyer F., Hubert F. Finite volume method for 2D linear and nonlinear elliptic problems with discontinuities. *SIAM Journal on Numerical Analysis*. **46** (6), 3032–3070 (2008).
- [22] Lahmi B., Rhoudaf M., Staïli N. Numerical analysis of a nonlinear discrete duality finite volume scheme for Leray–Lions type elliptic problems in Orlicz spaces. *Applied Numerical Mathematics*. **185**, 406–433 (2023).
- [23] Bazirha Z., Azrar L. Adaptive Finite Volume Schemes for Anisotropic Heterogeneous Diffusion Problems on Arbitrary Convex and Nonconvex Meshes. Submitted 2023.
- [24] Knabner P., Otto F. Solute transport in porous media with equilibrium and nonequilibrium multiple–site adsorption: uniqueness of weak solutions. *Nonlinear Analysis: Theory, Methods & Applications*. **42** (3), 381–403 (2000).
- [25] Coudiere Y., Pierre C., Rousseau O., Turpault R. A 2D/3D discrete duality finite volume scheme. Application to ECG simulation. *International Journal on Finite Volumes*. **6** (1), 1–24 (2009).

- [26] Quenjel E. H., Saad M., Ghilani M., Bessemoulin–Chatard M. Convergence of a positive nonlinear DDFV scheme for degenerate parabolic equations. *Calcolo*. **57**, 19 (2020).
- [27] Cances C., Guichard C. Numerical analysis of a robust free energy diminishing finite volume scheme for parabolic equations with gradient structure. *Foundations of Computational Mathematics*. **17** (6), 1525–1584 (2017).
- [28] Costa R., Clain S., Machado G. J. Finite volume scheme based on cell-vertex reconstructions for anisotropic diffusion problems with discontinuous coefficients. *ICCSA 2014: Computational Science and Its Applications – ICCSA 2014*. 87–102 (2014).

Схема DDFV для нелінійних параболічних задач реакції–дифузії на загальних сітках

Базірха З., Азрар Л.

Науково-дослідний центр STIS, M2CS, кафедра прикладної математики та інформатики, ENSAM, Університет Мохаммеда V, Рабат, Марокко

Ця стаття присвячена нелінійній анізотропній параболічній моделі виду $\partial_t C(u) - \operatorname{div}(\Lambda \nabla u) + R(u) = f$, де C , R , f і Λ — це відповідно: дві нелінійні функції, джерело і анізотропний тензорний коефіцієнт дифузії. Для дискретизації простору розроблено різні типи схеми дискретної подвійності скінченного об'єму (DDFV), що призводить до додатно визначених матриць жорсткості для дифузійного члена. Використовується загальна сітка та розглядається жорсткий анізотропний тензор із розривними ефектами. Розроблено неявну часову схему, а також метод Ньютона–Рафсона для розв'язування отриманої нелінійної системи. Розроблено ітераційний інкрементний підхід, що враховує ефекти анізотропії, розривів та нелінійності. Продуктивність поданих прямих і непрямих схем DDFV для різних сіток була продемонстрована різними чисельними тестами. Також продемонстровано суперзбіжність у дискретних L^2 та H^1 -нормах.

Ключові слова: *нелінійні параболічні задачі реакції–дифузії; анізотропний тензор; DDFV; метод Ньютона–Рафсона.*